

Optimisation of a Linearjet

Max Steden ¹, Jochen Hundemer ¹, Moustafa Abdel-Maksoud ¹

¹ Hamburg University of Technology (TUHH), Hamburg, Germany

ABSTRACT

The paper describes a method for carrying out an optimised design of a linearjet propulsor. It is expected that the propulsor will have high efficiency and good cavitation behaviour at a ship velocity range between 25 and 35 knots. By coupling an evolutionary optimisation algorithm with a tool for the generation of the propulsor geometry and its meshing as well as two flow-solvers, the design process occurs mostly automated. The investigated case shows a well performing propulsor at the simulations conditions. The comparison with results of measured open water tests and cavitation tests confirms the good characteristics of the developed propulsor.

Keywords

Multi-component propulsor, submerged waterjet, linearjet, optimisation, design procedure.

1 INTRODUCTION

Fast ships require efficient propulsors with low sensitivity to cavitation within their operation range. One of the most common propulsor for such velocities is the waterjet, which is a propulsor being integrated in the aft ship hull. Its propulsive efficiency decreases significantly at lower velocities. Up to a certain ship speed the most used propulsor is the conventional propeller. Comparing the propulsive efficiency η_D in Figure 1 shows that the conventional propeller performs well up to velocities around 25kn, while waterjets attain high efficiencies at more than 35kn. For each propulsor the figure shows upper and lower boundaries of realised propulsors with acceptable efficiency values.

Surface piercing propellers can be used in a velocity range higher than conventional propellers, but their applicability is restricted to small and medium boats. According to Faltinsen (2005), this kind of propulsor as well as supercavitating propellers are applicable at ship speeds beyond of 40kn.

Between the operational velocity ranges of conventional propellers and waterjet propulsors there is a field, where multi-component-propulsors appear to be advantageous. Such propulsor is called 'linearjet' in the present study. As to be seen in Figure 2, it consists of four components: rotor, hub, duct and stator.

In a certain way a linearjet can be treated as a combination of a conventional propeller and a waterjet. The water passes through it without being deflected or lifted to a higher level as in the case of the waterjet.

Therefore the theoretically attainable efficiency of a linearjet should be higher than that of the waterjet. The aim is to take advantage of this fact and, in analogy to the waterjet, to achieve an increased pressure level at the rotor-position in order to avoid cavitation. Raising the pressure level inside the propulsor, holds the risk of a raised rate of bypassing flow. In this case the propulsor could not perform satisfactorily, as the mass flow rate would decrease and the intended design point could not be reached. Contrary to the conventional propeller, the duct reduces the strength of the tip vortex and the stator helps to recover swirl energy from the rotor flow. These details provide good prerequisites for the design of a high-performance propulsor. As the interactions among the single components of the propulsor are quite complex, an appropriate technique has to be developed for the design of such a propulsor.

2 DESIGN CONCEPT

The aim of the present study is the development of an optimisation based design-procedure for a linearjet. To simplify the problem, the inflow is considered to be homogeneous. The inflow velocity, the total thrust and the rotor diameter are assumed to be known quantities. The procedure uses a parameterized geometry description of the propulsor consisting of relationally arranged components and automatic meshing tools. These are coupled with two numerical codes for potential and viscous flow. The codes are applied to calculate the hydrodynamic characteristics of the propulsor. In case of the potential flow, the procedure uses a first-order 3D-boundary-element method called IST-Hydro which was extended for the present study concerning the use of several propulsor components. The RANSE-calculations are performed by the commercially available numerical code ANSYS CFX.

The efficiency and the cavitation pattern are combined in one single target value. This value is used as the response to the optimisation method, which then generates a new set of geometric parameters. The optimisation method is based on a genetic algorithm.

Figure 4 shows a scheme of the whole design procedure. It consists of two stages within one loop (Pre-Optimisation) and a subsequent stage (Fine-Optimisation) after the loops' convergence.

In the first stage, the geometry of the rotor and stator are optimised to achieve high efficiency at lowest possible cavitation. The aim of the second stage is to achieve a

high pressure level inside the duct while the resistance of the duct must be kept as low as possible.

The design starts with the generation of a streamline around a hub using a simple RANSE-simulation. The exact geometry of the rotor in this stage is not considered but its effect on the flow is simulated by a body-force model. The estimated streamlines near the rotor tip are used to construct the first duct geometry. For a predefined duct thickness, the duct geometry can be constructed, which has a minimum disturbance on the flow. Now the duct geometry is passed to the pre-optimisation. In the first optimisation stage, a panel method is applied to determine the most efficient rotor and stator geometry for the desired thrust with optimum cavitation performance, while the duct and hub geometry is kept constant. In the next stage, axis-symmetric RANSE simulations are carried out to optimise the geometries of duct and hub while the rotor is still simplified by employing the body-force model. The circulation of the selected rotor geometry is used to prescribe the radial thrust distribution. The aim of this optimisation is to increase the pressure level inside the duct specially at the rotor location without having an over proportional increase of duct resistance. Increasing the pressure helps to avoid cavitation at the rotor within the next optimisation loops.

Figure 5 shows exemplarily the scheme of the RANSE-part of the pre-optimisation. The optimisation algorithm generates a set of parameters within given boundaries. This is passed to the interface, which starts to determine the polynom coefficients fulfilling the demanded geometrical conditions. These are included in a CAD-control script for a CAD-Program, which generates the mesh around the developed geometry. The mesh is configured with boundary conditions and used in the RANSE-solver coupled with the body-force-model. The result file of the RANSE-simulation is read by the interface and the target value is calculated for the current geometry. The target value is passed to the optimisation algorithm as the response to the set of parameters.

A pre-optimised geometry is being identified by applying both potential flow and RANSE methods iteratively. Subsequently, a fine optimisation takes place within closer limits of the variable parameters. Therefore, the RANSE solver is included again, evaluating the full discretised 3D geometry of all four components in a quasi-stationary numerical simulation. The commercially available code ANSYS TurboGrid is included for the generation of the mesh in the rotor- and the stator domain in this stage. Here, all components are varied simultaneously and all interactions are considered. The target value consists of the overall efficiency and the cavitation characteristics. This stage generates a fine-tuned geometry within closer geometric limits compared to the geometry achieved within the pre-optimisation.

To a great extent, the potential-part of the pre-optimisation and the one at the fine-optimisation follow the same steps. The main difference is the requirement of

a 2D boundary mesh for the potential method and two meshing tools used for different regions at the fine-optimisation.

2.1 Parameterisation of the Geometry

For a fast and reliable optimisation procedure, it is important to reduce the number of parameters for the geometry description to a minimum. The parameters should be able to describe all promising geometric measures to guarantee an efficient optimisation process. Hence the present study uses a holistic propulsor description oriented at the physical laws.

The construction of rotor and stator is based on the inner duct surface and the hub contour. The duct is described by its meanline z_M and the thickness distribution t_M by the following function using the coefficients z_{M1} to z_{M5} and t_{M1} to t_{M5} :

$$z_M = z_{M4}x^4 + z_{M3}x^3 + z_{M2}x^2 + z_{M1}x + z_{M0}$$

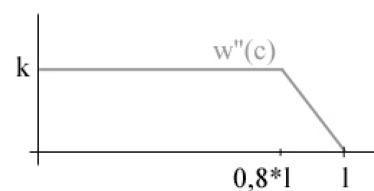
$$t_M = t_{M4}x^4 + t_{M3}x^3 + t_{M2}x^2 + t_{M1}x + t_{M0}\sqrt{x}$$

The coefficients are determined by solving a particular linear system of equations. At the ducts' meanline the radial position of the leading and the trailing edge are defined by a variable parameter describing the ratio of the propulsors inlet to outlet area A_E/A_A . Further two additional parameters give the gradient at these positions. Another variable value is given by the duct diameter at the axial position of the rotor, as this measure affects the pressure level at the rotor. The developed description allows the generation of ducts with different geometrical characteristics and pressure levels inside the propulsor.

The ducts' thickness distribution is generated as a ratio of the maximum thickness at a certain axial position and a measure for the bending circle at the leading edge.

When the duct and hub contour is defined, the propulsor's cross-sectional flow area at each axial position A is known. The profile baseline in figure 3 and 7 is a 3D-curve. It is constructed at the meridian contour depending on the defined mass flow Q , the area A and the turn rate of the shaft n . Presuming a known velocity distribution, the rotor profile-sections experience a resultant flow velocity vector c_1 in figure 8. The vector c_1 depends on the local flow velocity along the meridian and on the tangential velocity.

The camberline of rotor and stator is constructed by the function $w = f(c)$. The second derivative $w'' = f'(c)$ corresponds to a NACA Four-digit Section-Profile with a meanline $a = 0.8$:



Its definition range is divided into a part under and over a:

$$w''(0 \leq c \leq a) = k$$

$$w''(a \leq c \leq l) = k \cdot \left(1 - \frac{c-a}{l-a}\right)$$

This leads to the first derivative:

$$w'(0 \leq c \leq a) = \int_c w'' dc = kc$$

$$w'(a \leq c \leq l) = ka + \left(2 - \frac{c-a}{l-a}\right) \cdot \frac{k}{2} \cdot (c-a)$$

The numerical summation of the first derivative results in the rotors' meanline $w(c)$.

The double integral of the function leads to a maximum value $w(l) = w_{\max}$. This value is varied by the optimisation procedure at three radial positions. The relation between w_{\max} and k is:

$$k = \frac{2 \cdot w_{\max}}{a+l}$$

The velocity vector of the flow at the trailing edge c_2 is estimated based on the function w . The vector c_2 in the rotating coordinate system is transformed into the vector m in the stationary coordinate system. Analogous to the rotor, the stator mean line is constructed from this vector m , so that the flow after the stator's trailing edge is swirlfree.

From those mean lines, the thickness of a NACA Four-digit-Profile is set off.

Apart from the radially variable value w_{\max} , the optimising procedure varies the chordlength and the pitch at the same radial positions. The pitch is differed by a factor w_{fact} changing the vector c_1 . By this factor the pitch can be changed independently of camber and chordlength values.

This geometry description allows a variation of parameters influencing the hydrodynamic characteristics of the propulsor directly.

3 INVESTIGATED CASE

As the described propulsor is dedicated for a velocity range between conventional propellers and waterjets, a ship at 27.5kn was exemplarily chosen to test the method. It is a wide twin screw ship which had been investigated at model scale (Schmiechen & Kracht 1996). The main dimensions of the ship are $L_{pp} = 90\text{m}$, $B = 12.78\text{m}$, $T = 3.651\text{m}$ and $\nabla = 2187\text{m}^3$. For the full scale ship at this velocity the determined total thrust was 998.2kN. The propeller diameter was 3.215m. The calculations were all realised in full scale. The goal of the investigation was the generation of a cavitation free propulsor for this ship at its operation point.

3.1 Optimisation

The duct was generated with the help of the coordinate of the streamline passing at the rotor radius position, see figure 6. The illustrated plane shows the dimensionless velocities around the components resulting of a simple RANSE-simulation. Instead of the rotor the body-force model was used in the simulation as to be noted by the elevated velocities shown in the darker contours.

The optimisation procedure generates a high number of different geometries which can be treated statistically. The geometry with the lowest target value forms the best adapted propulsor for the given boundary conditions. All variable parameters were checked concerning their boundaries. In case that the results of the optimisation method are concentrated near certain given boundaries (limits of a control parameter for the geometry), this boundary should be extended to allow more geometrical variations.

Figure 10 depicts each of 400 evaluated geometries with a targetvalue better than zero. Each investigated geometry is represented by one point. The figure shows the targetvalue of the geometries with respect to two radial positions over the chordlength at a nondimension radius 0.5 and 1. The values vary towards a certain optimal range within the total boundary range. The $r/R=0.5$ position chord(05) shows a smaller optimum range close to the upper boundary, however the tip-position chord(1) reaches close-to-optimum values within the upper half of its variation range. The dash-marked points show the particular value of the best evaluated geometry.

Figure 11 shows the realised pitch values of the same geometries. The pitch at $r/R=0.5$ tends towards higher values with just one exception. The optimum geometry was found at a high pitch-value as to be expected. The pitch at the blade-tip forms its optimum at lower values. The optimum was found at about one third of the variation range.

The camber at the position $r/R=0.5$ in figure 12 shows a clear tendence towards its optimum at the highest dash-marked value. At the tip-position, lower camber values result to lead to the optimal geometry.

The optimised geometry was achieved by several iterations amongst the potential-based and the RANSE-based pre-optimisation. The results of the potential method in figure 9 are shown as velocities at the propulsors surface, whereas the optimisation method uses just integral values of thrust and torque.

The planes in figure 13 show dimensionless velocities around the propulsor, determined by the RANSE-Solver. The local pressure is depicted at the propulsors surface.

The pressure distribution at the propulsor surface, shown in figure 14, was achieved by a unsteady RANSE-simulation, which was performed for the selected geometry to validate the other used methods. The values in the figure are normalized by the stagnation pressure.

3.2 Verification with Experimental Data

The optimised linearjet was investigated experimentally at the Potsdam Model Basin (SVA Potsdam). Open water and cavitation tests were carried out. The maximum efficiency in the model scale is 0.6428.

The measured values were extrapolated to full-scale. The extrapolation is based on factors for considering the scale effect which was determined by RANSE-calculations for the developed geometry as functions of the advance ratio. The full-scale efficiency is 0.7216.

The numerical results of the RANSE-calculation for full-scale and the extrapolated experimental data shown in figure 15 match quite well throughout the range of advance ratios $0.4 \leq J \leq 2.7$. The efficiency (η) was overestimated by about 2.5% by the RANSE-calculations. The thrust-coefficient K_T and the torque-coefficient K_Q agree very well at the operation point of $J=1.65$.

Figure 16 shows the cavitation characteristics of the linearjet. At the operation point, cavitation occurs just in the gap region between rotor and inner surface of the duct. BSSK means the begin of cavitation at the suction side, whereas the BSWK-curve shows the begin of tip vortex cavitation.

The experimental data confirm that the applied numerical method provides reliable results and it is suited to generate an optimised propulsor for real full size geometries.

CONCLUSION

The experimental and the numerical results show that the development of a high efficient propulsor for a ship velocity range above 25 knots is possible. In comparison with the conventional propeller, the linearjet has some important advantages. The range of operation with the

high efficiency is wide, so that by a change of the operation point no dramatic loss of the propulsive efficiency takes place. The cavitation pattern can be reduced or eliminated. That means less vibration and erosion problems.

REFERENCES

- Faltinsen, O.-M. (2005). 'Hydrodynamics of High-Speed Marine Vehicles'. Cambridge University Press, UK.
- Hundemer, J., Naujoks, B., Hachmann, T., & Abdel-Maksoud, M. (2006), 'Auslegung von Schiffspopellern mit evolutionaeren Algorithmen'. Schiffbautechnische Gesellschaft, Hauptversammlung, Hamburg, Germany.
- Juergens, D. & Heinke, H.-J. (2006), 'Untersuchung tiefgetauchter Waterjets', Schiffbautechnische Gesellschaft, Hauptversammlung, Hamburg, Germany.
- Kerwin, J.E. (2006). 'Hydrodynamic issues in waterjet design and analysis'. Presentation, Office of Naval Research, 26th Symposium on Naval Hydrodynamics, Rome, Italy.
- Kim, K.-H. (2006). 'Waterjet Propulsion for High-Speed Naval Ships'. Advanced Naval Propulsion Symposium, Arlington, Ballston.
- Schmiechen, M. & Kracht, A. (2003). 'Erweiterung der D-Serie: Breite, schnelle Zweischraubenschiffe', Abschlußbericht Nr.: 1267/96, Versuchsanstalt für Wasserbau und Schiffbau, Berlin, Germany.
- Steden, M., Hundemer, J., Mueller, S.-B. & Abdel-Maksoud, M. (2007), 'Geometrische Parametrisierung und Untersuchung der Umstroemung von aus Mehrkomponenten bestehenden Schiffsantrieben'. Jahrbuch der Schiffbautechnischen Gesellschaft.

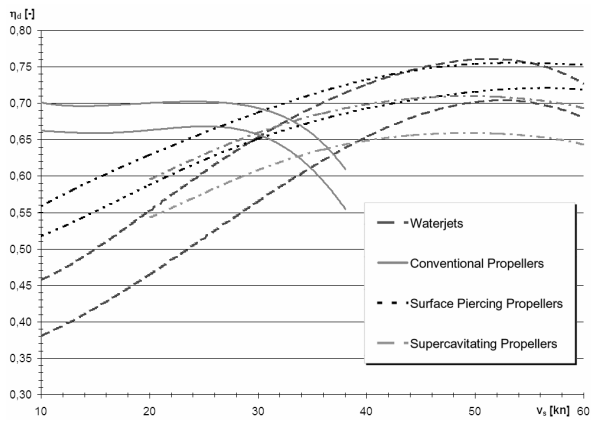


Figure 1: Propulsive efficiency of different propulsors according to Kim (2006)

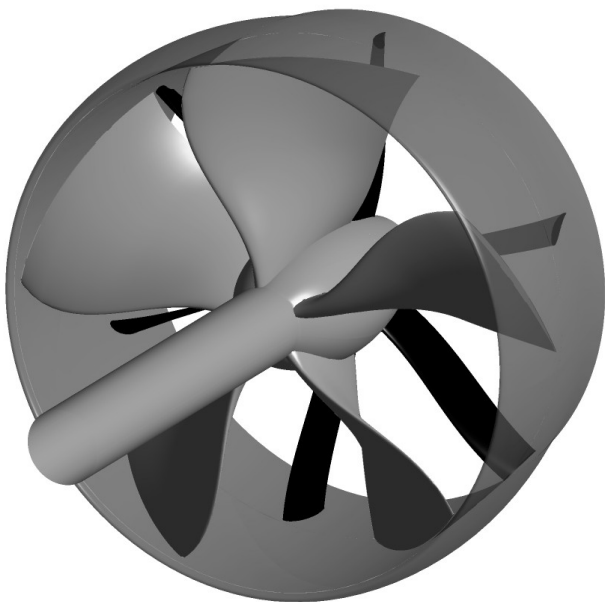


Figure 2: 3D-view of a linearjet-geometry

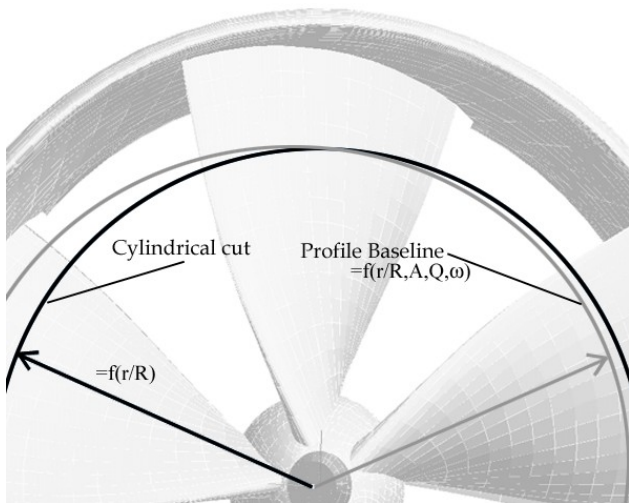


Figure 3: Profile Baseline in axial view

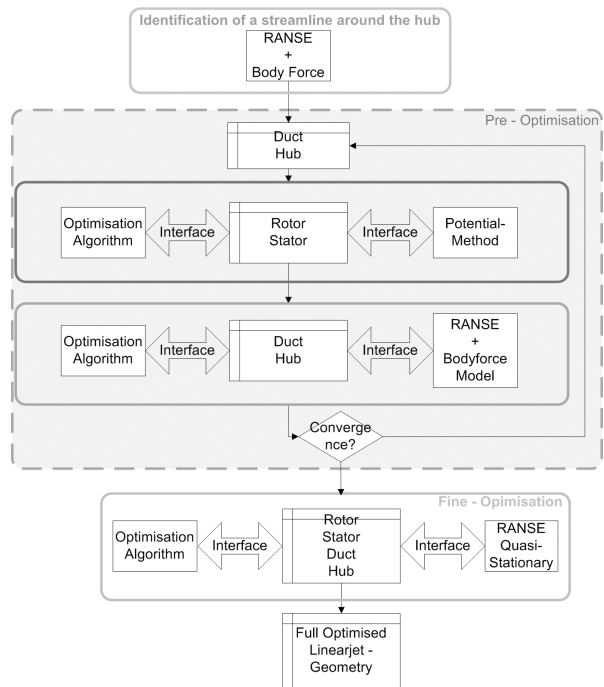


Figure 4: Design procedure

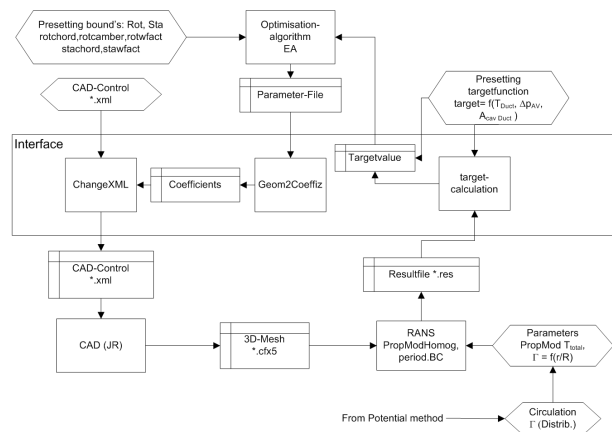


Figure 5: RANSE-part of the pre-optimisation

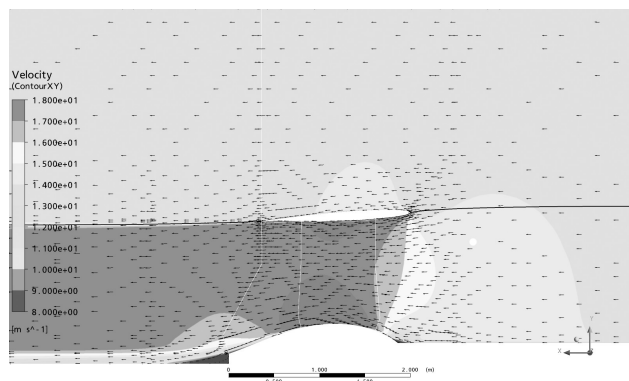


Figure 6: Duct constructed along a streamline

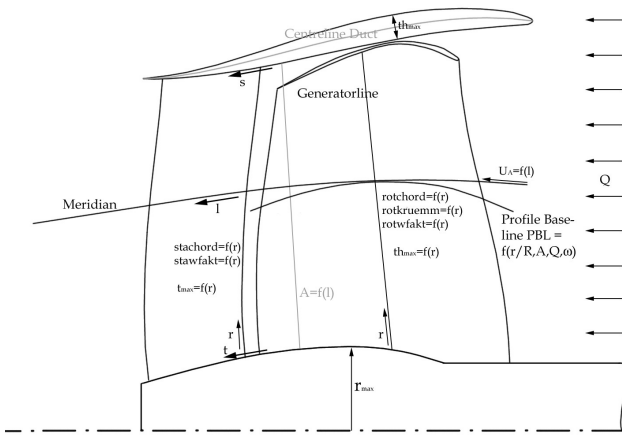


Figure 7: Scheme of the linearjet construction

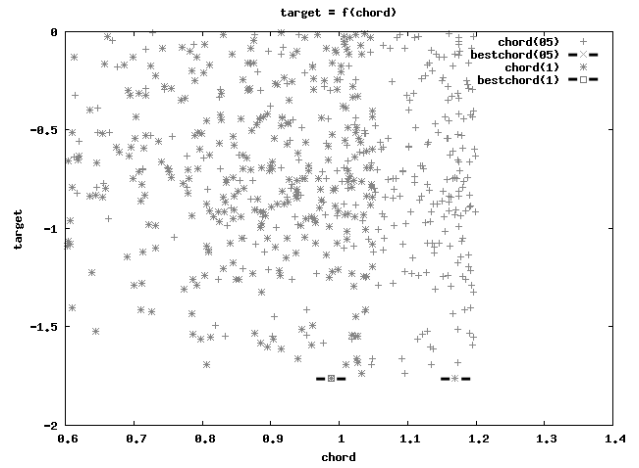


Figure 10: Development of the chordlength

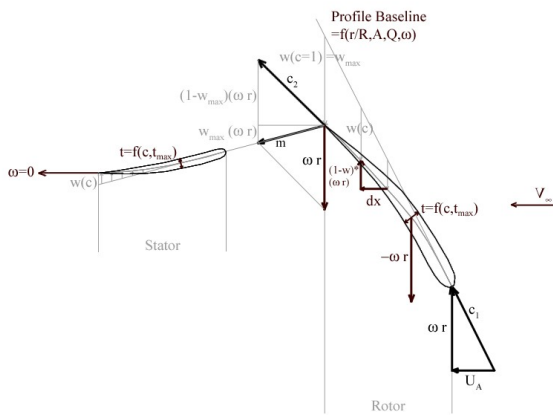


Figure 8: Profiles relative to the profile baseline

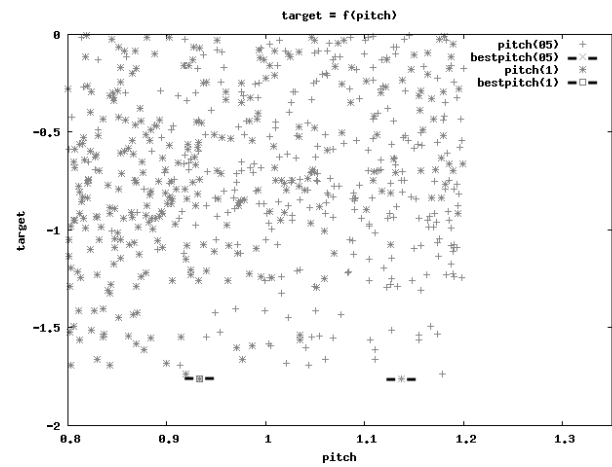


Figure 11: Development of the pitch

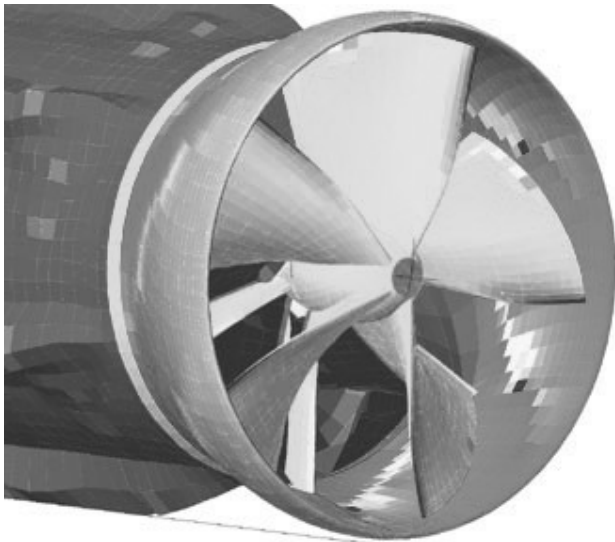


Figure 9: Velocities according to the potential flow

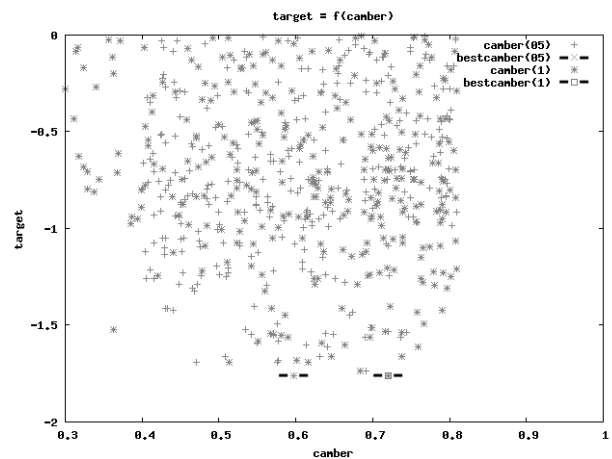


Figure 12: Development of the camber

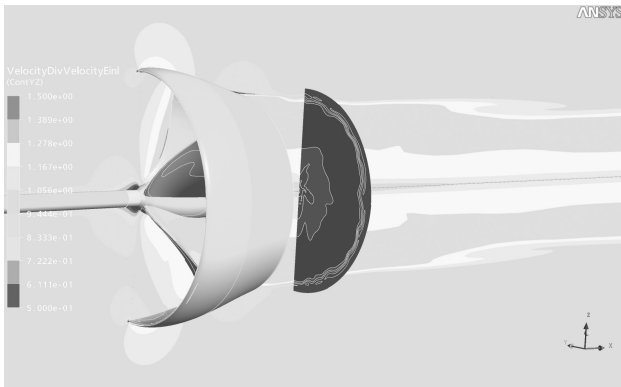


Figure 13: Dimensionless velocities around the Linearjet

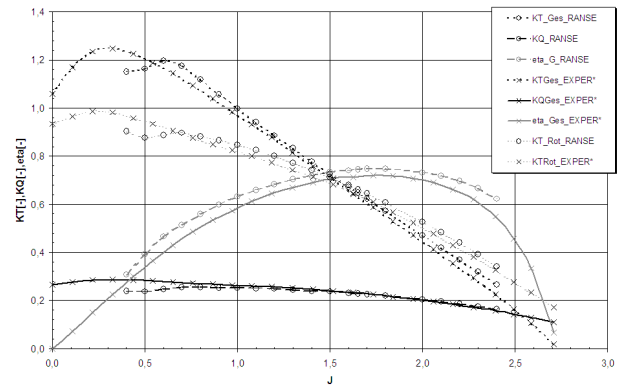


Figure 15: Open Water Diagram: Comparing RANSE-Simulation with experimental data (EXPER)

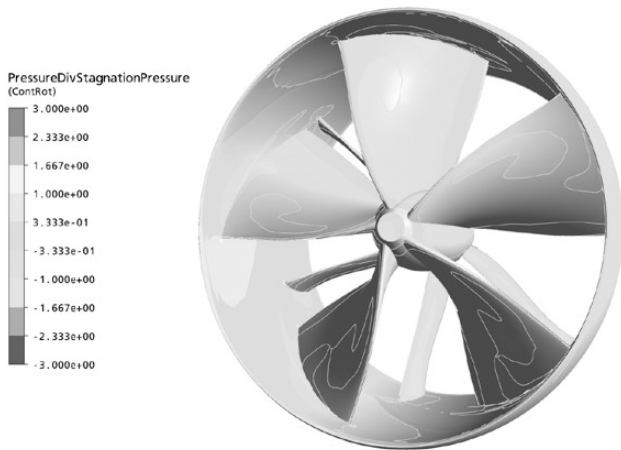


Figure 14: Dimensionless pressure on the propulsor

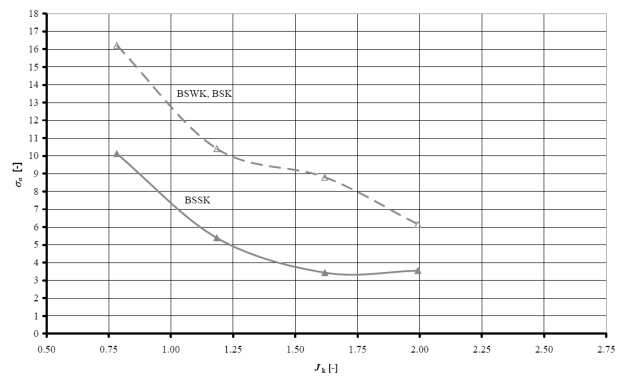


Figure 16: Cavitation characteristics of the linearjet